Modeling contamination migration on the *Chandra X-ray Observatory* — IV

Stephen L. O'Dell[*] [a], Douglas A. Swartz [b], Neil W. Tice [c], Paul P. Plucinsky [d], Herman L. Marshall [c], Akos Bogdan [d], Catherine E. Grant [c], Allyn F. Tennant [a], and Matthew Dahmer [e]

[a] NASA Marshall Space Flight Ctr., MSFC/ST12, Huntsville, AL 35812, USA
[b] Universities Space Research Assoc., MSFC/ST12, Huntsville, AL 35812, USA
[c] Massachusetts Institute of Technology, 77 Massachusetts Ave., Cambridge, MA 02139, USA
[d] Smithsonian Astrophysical Observatory, 60 Garden St., Cambridge, MA 02138, USA
[e] Northrop Grumman, MS33, 60 Garden St., Cambridge, MA 02138, USA

ABSTRACT

During its first 18 years of operation, the cold (about -60°C) optical blocking filters of the Advanced CCD Imaging Spectrometer (ACIS), aboard the *Chandra X-ray Observatory*, has accumulated a growing layer of molecular contamination, which attenuates low-energy x rays. Over the past several years, the accumulation rate, spatial distribution, and composition have changed. This evolution has motivated further analysis of contamination migration within and near the ACIS cavity, in part to evaluate potential bake-out scenarios intended to reduce the level of contamination. This paper, the fourth on this topic, reports the results of recent contamination-migration simulations and their relevance to a decision whether to bake-out the ACIS instrument.

Keywords: X-ray astronomy, CCDs, contamination, modeling and simulation, spacecraft operations

1. INTRODUCTION

Since the launch in 1999 of the *Chandra X-ray Observatory*[1,2,3,4], the low-energy (< 1 keV) response of its Advanced CCD Imaging Spectrometer[5,6] (ACIS, Figure 1) has continued to decline, due to a growing layer of molecular contamination on its cold (≈ -60°C) optical blocking filters (OBFs). Based upon the observed attenuation of low-energy x rays[7,8] (§2), the cold (≈ -60°C) surfaces in the ACIS cavity (Figure 1) have thus far accumulated 250–500 μg cm^{-2} of unidentified molecular contamination[9] over 18 years of operation. This mass column is 100 times pre-flight estimates and 10 times that of the OBFs themselves. Nonetheless, the total mass of condensed contaminants is calculated to be < 1 g, a small fraction of the *Observatory*'s 4800-kg mass.

The evolution (§2.1) of the x-ray absorption depth indicates changes in rate, gradient, and composition of the contaminants, which have markedly accelerated since about 2010. This increased rate of accumulation is plausibly related to temperature changes (§2.2) within the *Observatory*'s interior ("cavity"), resulting from overall warming due to degradation of the thermal multi-layer insulation (MLI) enveloping it.

In order to simulate accumulation of molecular contamination on the OBFs and potential bake-out scenarios, we developed and continue to refine the *Chandra* contamination-migration model (CCMM, §3). The CCMM comprises three related models: A geometric model (§3.1); a thermal model (§3.2); and a molecular-transport model (§3.3). As the methodologies for constructing these models were discussed in the previous papers[10,11,12] of this series, the current paper describes updates to the models and to model parameters.

For a range of volatilities, we have used the CCMM to simulate the accumulation of molecular contamination during normal operations, its vaporization for some bake-out scenarios, and its re-accumulation following an incomplete bake-out. Some examples of these simulations (§4) illustrate the sensitivity to the volatility of the unidentified contaminants.

[*] Contact author (SLO): stephen.l.odell@nasa.gov; voice +1 (256) 961-7776; fax +1 (256) 961-7522
Postal address: NASA/MSFC/ST12; 320 Sparkman Drive NW; Huntsville, AL 35805-1912, USA

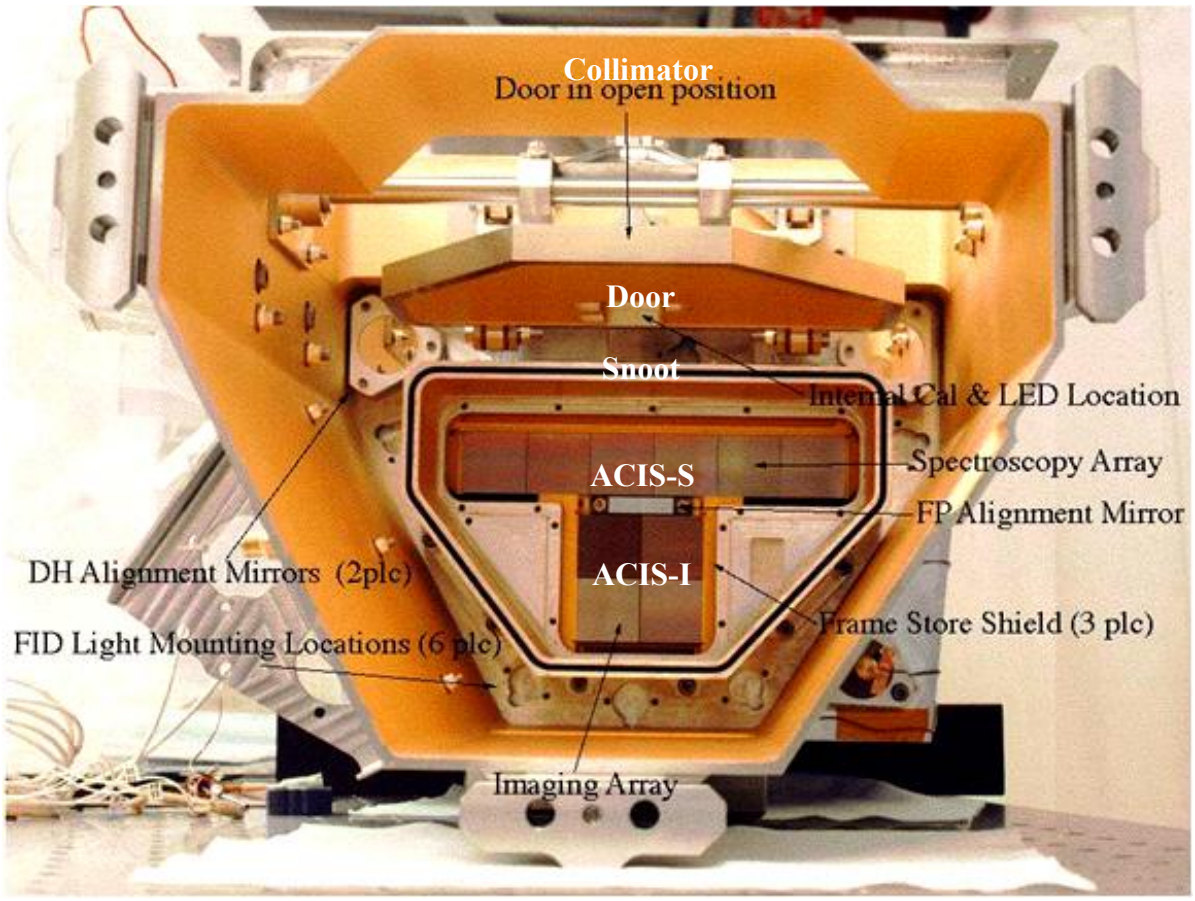

Figure 1. Top view of the engineering unit of *Chandra*'s Advanced CCD Imaging Spectrometer (ACIS), showing the 2×2-CCD ACIS-I and the 1×6-CCD ACIS-S focal planes. In the flight unit, aluminized-polyimide optical blocking filters OBF-I and OBF-S cover the I and the S focal planes, respectively. The OBFs lie within the "snoot" (with door opened since on-orbit check-out), which in turn lies within the ACIS "collimator" that envelopes the ACIS cavity.

We conclude (§5) with a summary of results and limitations of the CCMM simulations, plus a brief report on the current status of a bake-out decision whether to the *Chandra* ACIS. Spoiler alert: The *Chandra* Team has decided to defer a decision on the bake-out.

2. MEASUREMENTS OF OBF CONTAMINATION

Chandra's on-orbit calibration program monitors the evolution of the molecular contamination[13,14] on the ACIS OBFs. This section reports updated measurements of the evolution of the molecular contamination (§2.1) and notes a possible relationship between changes in the accumulated contamination and temperature changes (§2.2) within the *Observatory*'s cavity.

2.1. Observed evolution

Various ACIS spectrometric and LETG/ACIS-S high-resolution spectroscopic observations measure x-ray absorption by contamination accumulated on the ACIS OBFs. Figure 2 displays the evolution of the 0.66-keV absorption depth, inferred from ACIS-I and ACIS-S spectrometric measurements of the galaxy cluster Abell 1795 (A1795). Figure 3 shows the evolution of the molecular contamination on OBF-S, based upon high-resolution spectroscopy of the (non-thermal) blazar Markarian (Mrk) 421, using *Chandra*'s LETG/ACIS-S.

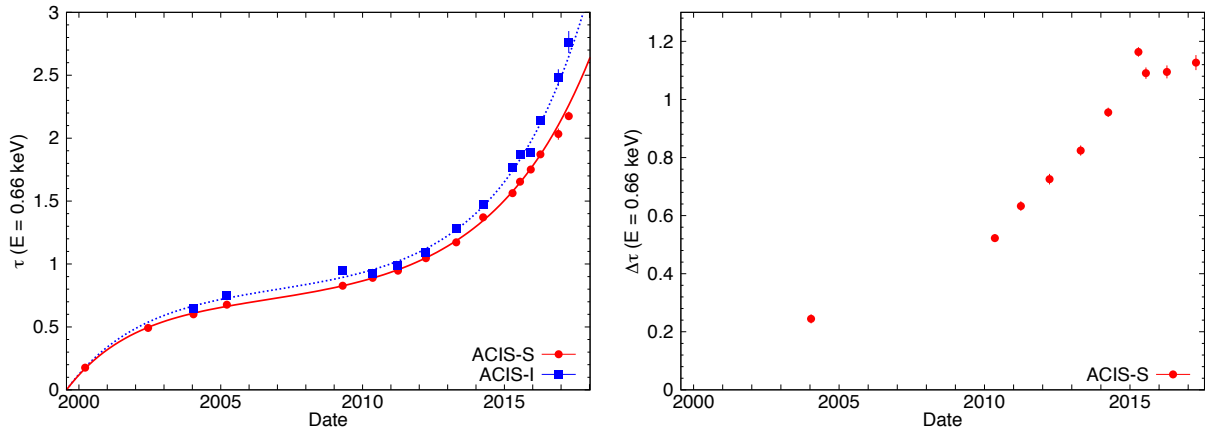

Figure 2. Evolution of the 0.66-keV absorption depth $\tau_{0.66}$ in molecular contamination on the ACIS optical blocking filters, as determined from observations of A1795. Left panel displays the temporal dependence of $\tau_{0.66}$ at the centers of OBF-S and of OBF-I. Right panel shows the temporal dependence of the center-to-edge difference in absorption depth $\Delta\tau_{0.66}$ for OBF-S.

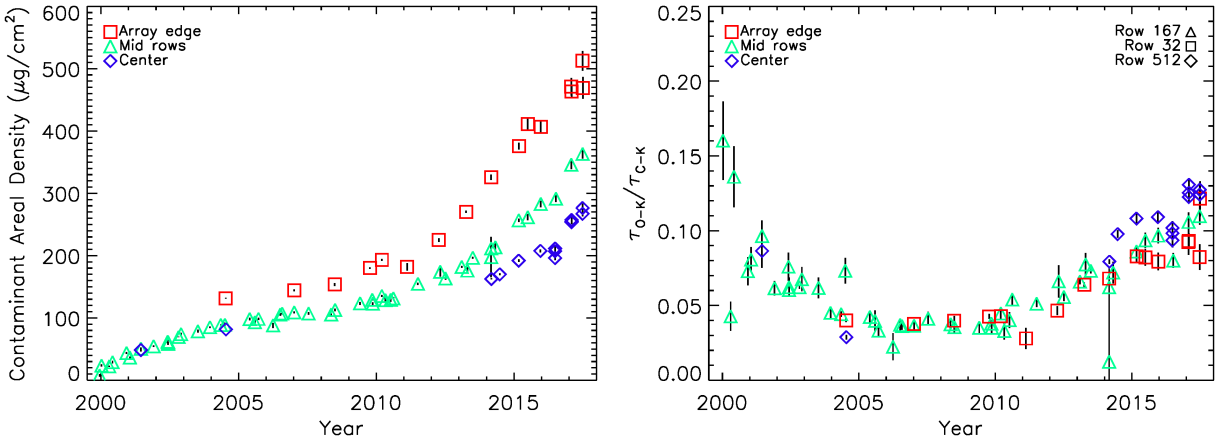

Figure 3. Evolution of the molecular contamination on OBF-S, as determined from LETG/ACIS-S spectroscopy of Mrk 421. Left panel shows the accumulated mass column—primarily carbon—near the array center (blue diamonds), near the array edge (red squares), and in between (green triangles). Right panel displays the ratio of the K-edge absorption depth for oxygen ($\tau_{O\text{-}K}$) to that for carbon ($\tau_{C\text{-}K}$) at the same locations.

The salient features of the observed evolution (Figure 2 and Figure 3) of the molecular contamination are then these:

1. Accumulation of molecular contamination started near the beginning of the mission.
2. The accumulation rate decreased steadily from the start of science operations in late 1999 until about 2010.
3. The accumulation rate increased again around 2010.
4. Accumulation is significantly larger near the edges of the OBFs than near their centers.
5. The composition of the accumulated contamination has evolved. (NB: Besides measuring C-K and O-K edges, the LETG/ACIS-S spectroscopy also detects the fluorine F-K edge but does not find the nitrogen N-K edge.)

2.2. Temperature changes

Temperature is of paramount importance in molecular contamination. For temperatures and volatilities relevant to molecular contamination of the ACIS OBFs, a 10°C increase raises (off-gassing or out-gassing) vaporization rates by roughly an order of magnitude. Consequently, temperature changes occurring about 2010 are suspect, when attempting to account for the increased accumulation rate on the OBFs at about that time.

Recall that the accumulation rate onto a surface equals the deposition rate (from other surfaces or sources) minus the vaporization rate from that surface. As contamination sources eventually deplete, an expected decline in the deposition rate naturally accounts for the early decrease in the accumulation rate onto the OBFs. However, the rise in the accumulation rate starting around 2010 requires either an increased deposition rate—e.g., a new or stronger source—or a decrease in the vaporization rate of contamination on the OBFs. The former explanation—increased deposition rate—naturally occurs if temperatures of other surfaces were raised. The latter explanation—decreased vaporization rate—could occur if the OBF temperatures were lowered.

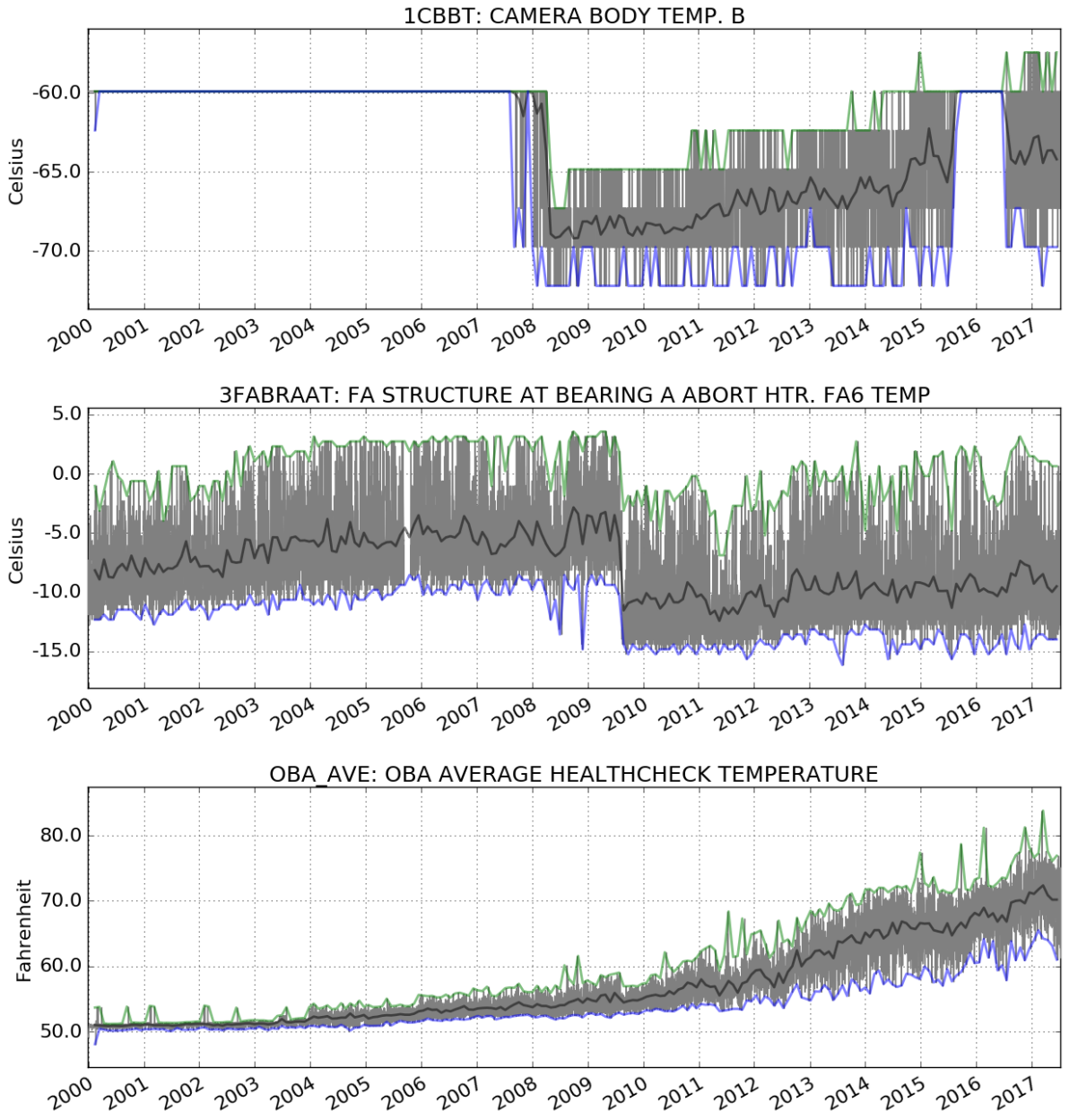

Figure 4. Recorded temperatures of the ACIS camera body (top panel), of a location in the translation table between the ACIS cavity and the Optical Bench Assembly (OBA) cavity (middle panel), and of the OBA itself (bottom panel).

Figure 4 shows that both types of temperature change have occurred: Turning off the detector-housing heater camera top in 2008 lowered the temperature of the camera body (top panel), which is now trending back toward its original controlled temperature (-60°C) as the *Observatory* continues to warm; the gradual loss of thermal control of the OBA has resulted in its continued warming (bottom panel), thus far by about 10°C. The first trend would tend to decrease the vaporization rate from the OBF; the second trend would tend to increase the deposition rate onto the OBF, due to increased out-gassing or off-gassing from warming surfaces within the OBA cavity. However, quantitative assessments of the importance of these two trends hinges upon the volatility properties of the contamination, which remain unknown.

3. MODELS WITHIN THE CCMM

The *Chandra* contamination-migration model (CCMM) comprises three related models: A geometric model (§3.1); a thermal model (§3.2); and a molecular-transport model (§3.3). As the previous papers in this series discuss the methodologies underlying these models, we here describe updates to the models and model parameters.

3.1. Geometric model

Figure 5 displays the geometric model employed in the current study. The main improvement in the geometric model is incorporation of additional detail for the structure—the translation table and "stove pipe"—connecting the ACIS cavity to the OBA cavity. The motivation for adding detail here was the recognition that this conduit is the coldest region of the *Observatory* cavity during a bake-out. Consequently, it throttles transport and venting of the molecular contamination.

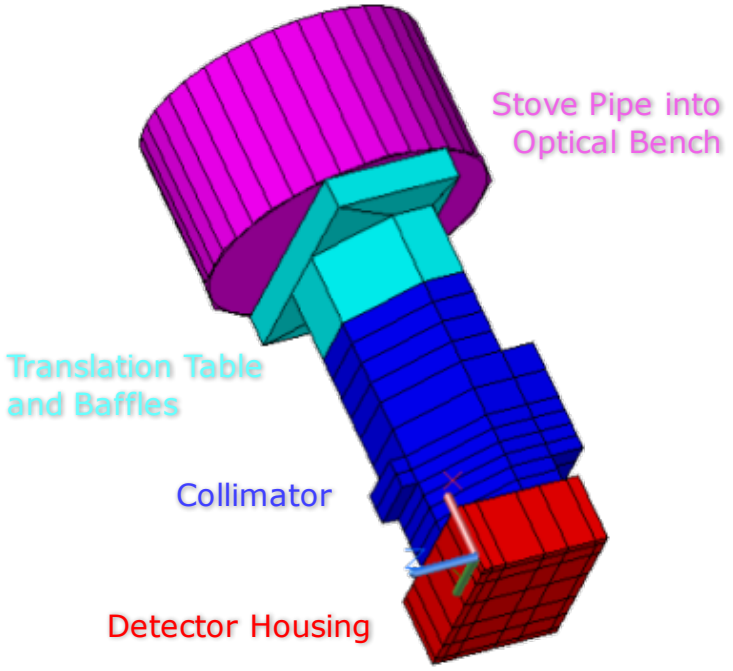

Figure 5. Geometric model used for the thermal analysis and for the molecular-transport analysis in the current study.

The new geometric model retains fine-scale resolution where important—738 nodes within the ACIS cavity, including 121 OBF-I and 203 OBF-S nodes—while reducing the model above the Stove Pipe to a simple Telescope Closeout, with straightforward coarse-scale boundary conditions. As with the previous study, we utilized the software tool Thermal Desktop™ (C&R Technology) and its RADCAL sub-module to calculate vector surface areas (A_j) and geometric view factors (f_{jk}), which govern either radiative or molecular transport from each surface element to the remaining surface elements.

3.2. Thermal model

In addition to the areas and view factors from the geometry model (§3.1), the thermal analysis requires specification of the radiative emissivity ε_j for each surface element, conductive linkages amongst elements, and thermal boundary conditions. Figure 6 and Figure 7 display the temperature distributions over the ACIS exterior and interior, respectively, during normal operating conditions (left panel) and during a room-temperature bake-out (right panel). For clarity, these figures do not display the conduit structure (translation table and stove pipe of Figure 5) between the ACIS and the OBA.

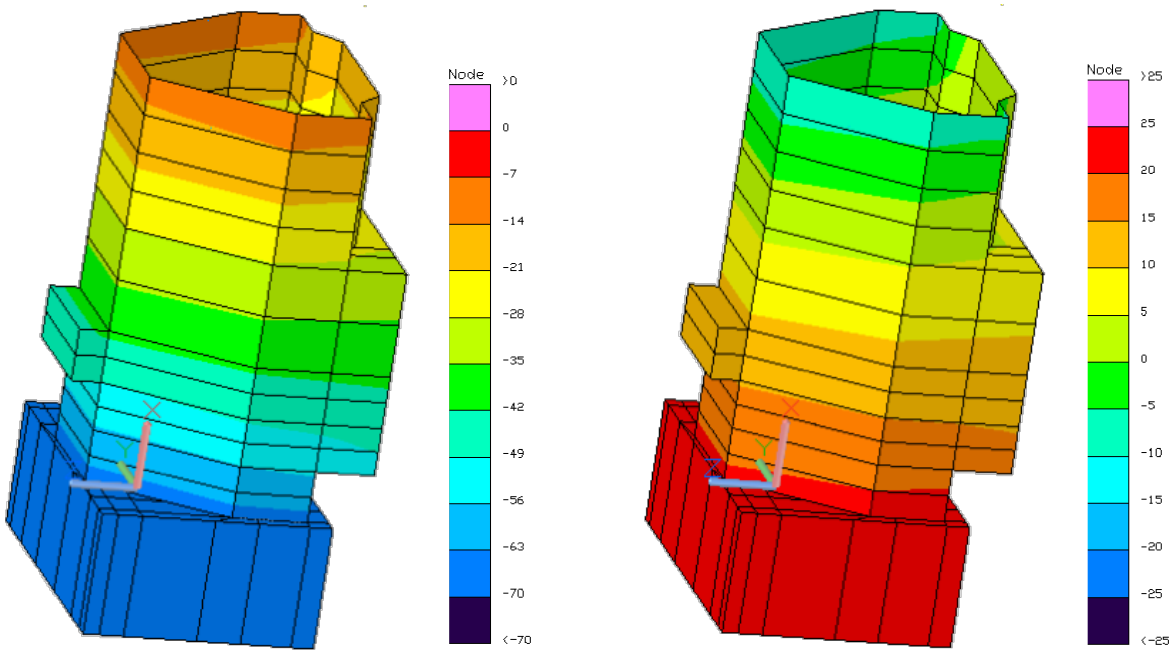

Figure 6. Temperature distribution over the exterior of the ACIS instrument during normal operations (left panel) with the detector heater off; during a room-temperature bakeout (right panel).

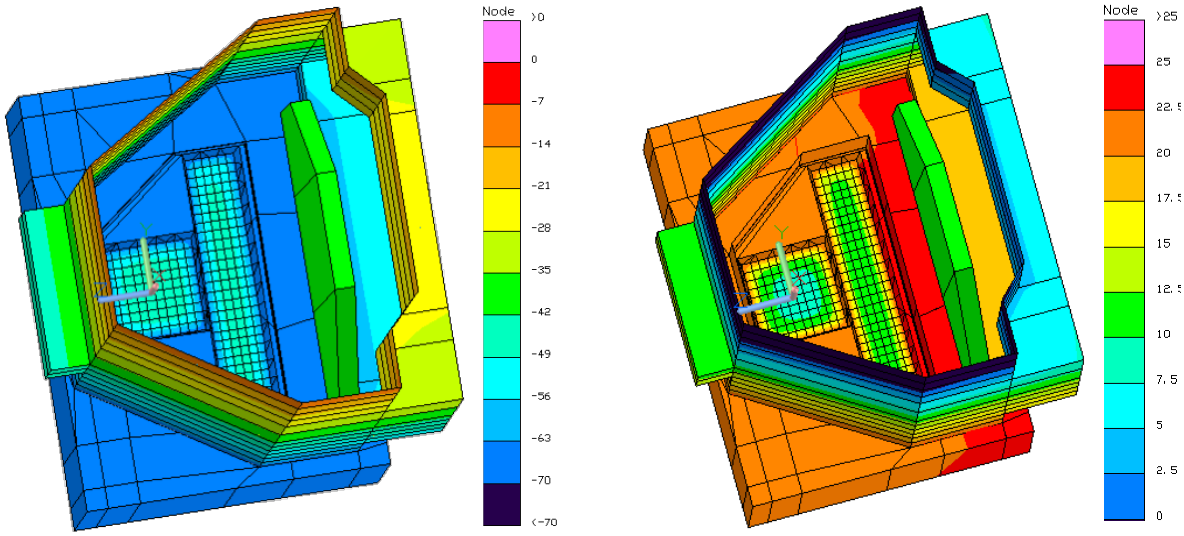

Figure 7. Temperature distribution over the interior (cavity) of the ACIS instrument during normal operations (left panel) with the detector-housing heater off and the focal-plane at -120°C; during a room-temperature bakeout (right panel) maintaining a cool (<-60°C) focal-plane.

As the ACIS camera body, OBF frames, and snoot are aluminum and tightly linked conductively, these structures are nearly isothermal at the camera-body temperature, which is recorded onboard (Figure 4). Consequently, the temperature at the OBF edges is well-determined, either during normal operations or during a bake-out, for which heaters would hold the temperature of the detector housing (camera body) at a set point. In contrast, the temperature near the OBF centers depends primarily upon radiative coupling of the OBF to the focal-plane below and to the *Observatory* cavity above. The latter coupling is sensitive to the radiative emissivity of the contaminated surface of the OBF, which we take $\varepsilon_{OBF+} \approx 0.4$—much higher than $\varepsilon_{OBF-} \approx 0.05$ for the pristine aluminized surface facing the focal plane.

For the room-temperature bake-out, we are now considering only scenarios that maintain a cool (<-60°C) focal-plane temperature. The motivation for this constraint is to minimize reverse annealing[15] of the proton-damaged front-illuminated CCDs, which could further increase their charge-transfer inefficiency (CTI), thus degrading their energy resolution.

3.3. Molecular-transport model

Using methods analogous to those used for radiative transport in the thermal analysis and essentially the same geometric model for the optical cavity, the molecular-transport model follows the exchange of molecular contamination amongst the surfaces—including sources and sinks (vents)—in the *Observatory* cavity. For purposes of illustration, Figure 8 shows the strong temperature dependence of the mass vaporization rate $\dot{\mu}_v$ of several example organic compounds. This rate is simply related to the vapor pressure P_v, which follows the Clausius-Clapeyron relation:

$$\dot{\mu}_v(T) = \frac{P_v(T)}{\sqrt{2\pi\, R\, T/M}} = \dot{\mu}_v(T_0)\sqrt{\frac{T}{T_0}}\exp\left[-\frac{\Delta_v H}{R}\left(\frac{1}{T}-\frac{1}{T_0}\right)\right],$$

with R the ideal gas constant, T_0 a reference temperature, M the molar mass of the contaminant, $\Delta_v H$ its vaporization (evaporation or sublimation, as appropriate) enthalpy.

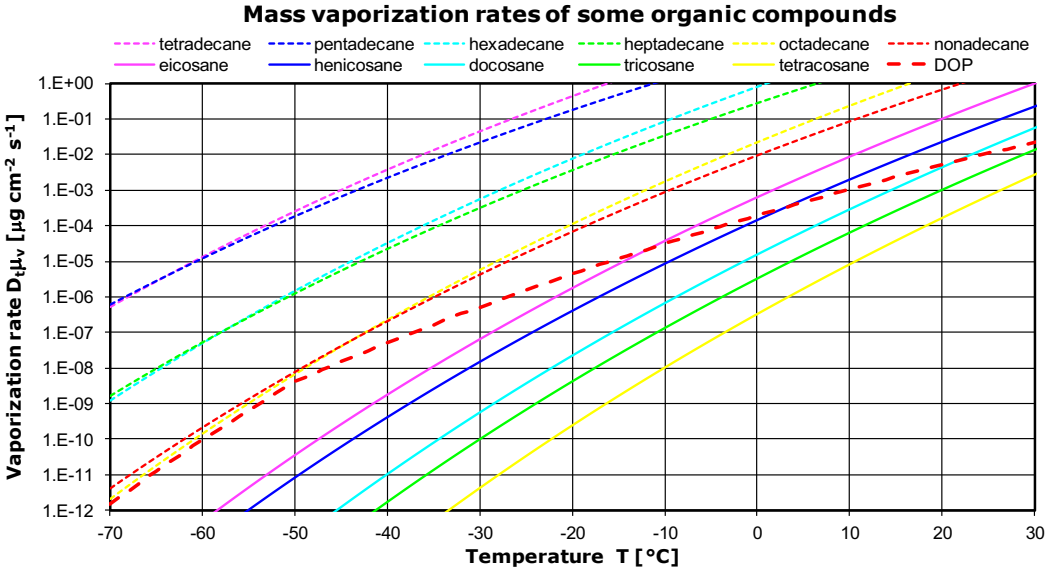

Figure 8. Temperature dependence of the mass vaporization rate of several simple organic compounds. Note the strong dependence upon temperature, which is related to the vaporization enthalpy of the compound[16].

4. CCMM SIMULATION EXAMPLES

LETG/ACIS-S spectroscopy provides information[9,14] on the mass column and ratio of atomic constituents (C, O, and F)—including the ratio of aromatic (double) to aliphatic (single) carbon bonds—of the contaminants on the OBFs. However, these data are insufficient to identify the specific molecular species contributing to the contamination.

Without identification of the specific contaminants and, hence, their vaporization properties, CCMM simulations—even if the models were perfect—cannot lead to a definitive assessment of the likelihood for a successful bake-out of the ACIS OBFs. Figure 9 demonstrates the sensitivity of the bake-out simulation to the temperature dependence of the vaporization rate, comparing results for octadecane (left panel) and those for dioctyl phthalate (DOP) or diethyhexyl phthalate (DEHP), a well-known plasticizer (right panel). As Figure 8 shows, these two molecules have nearly identical vaporization rates below -50°C, the melting point for DOP; however, above -50°C, the evaporation rate of (liquid) DOP (dashed red line) rises substantially more slowly with temperature than the sublimation rate of (solid) octadecane (solid yellow line). Consequently, although the volatilities of the two molecules are nearly indistinguishable at OBF operating temperatures, a successful bake-out would require about 40 times longer for DOP than for a contaminant with vaporization properties similar to those of octadecane.

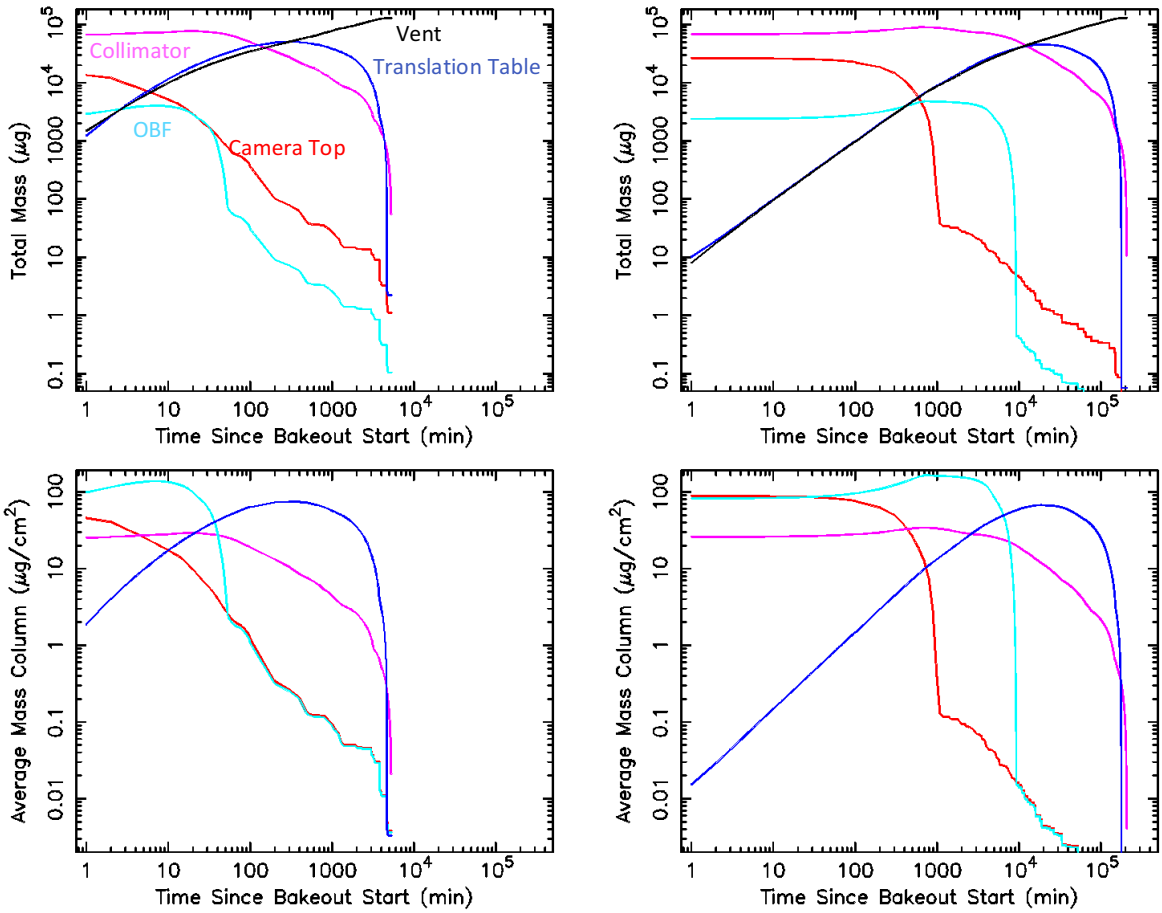

Figure 9. CCMM simulations for an ACIS room-temperature (+25°C) bake-out with a cool focal-plane temperature (-60°C), for two example contaminants (see text). Top panels plot the total contaminant mass on each structure; bottom panels, the average mass column on each. Left panels assume approximate vaporization rates of octadecane; right panels, vaporization rates of dioctyl phthalate. (NB: The ragged decline at low mass columns is an artifact of the numerical method.)

For purposes of discussion, we would regard a bake-out as fully successful if it totally vents the contaminants to space; partially successful if it completely cleans the OBFs without total venting. As evidenced by the simulation examples in Figure 9, we must face the possibility that a bake-out might not be fully or even partially successful. Consequently, we have begun simulating re-deposition of molecular contamination after a partially successful bake-out.

Figure 10 displays the results for a simulation of post-bake-out re-accumulation, following a partially successful 3-orbit (8-day) bake-out of an example contaminant with a vapor pressure one-tenth that of octadecane. Starting with an average mass column of 250 μg/cm^2 on the OBFs, the simulated bake-out completely cleaned the OBFs and vented 86% of the

contaminant to space. About two-thirds the unvented contamination redeposited onto the OBFs within 100 days, resulting in a 25 μg/cm^2 mass column. NB: The post-bake-out simulation treated only re-deposition of contamination already in the ACIS cavity and translation-table extension, neglecting continuing contamination from sources outside the stove pipe.

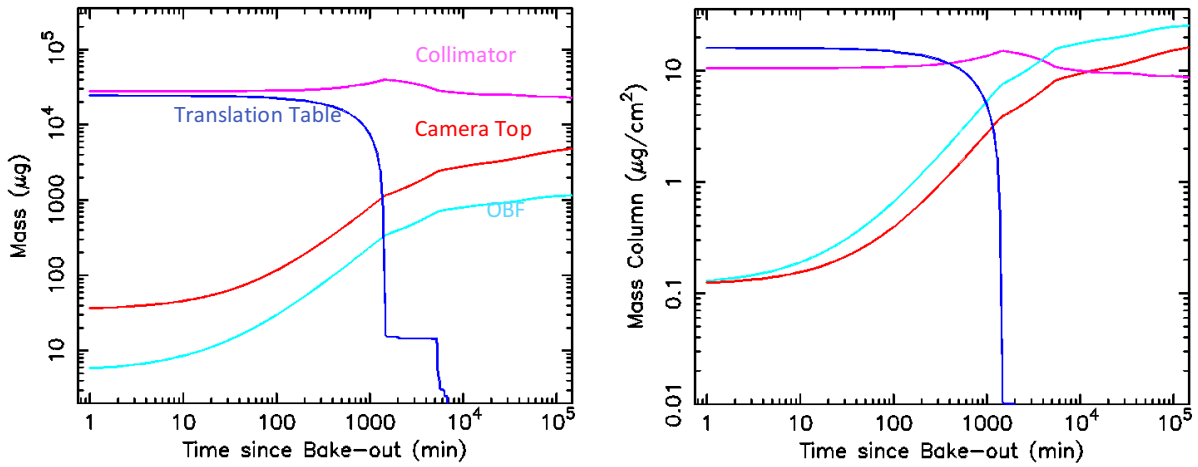

Figure 10. CCMM simulations for contamination re-accumulation after a partially successful ACIS room-temperature bake-out, showing the re-accumulated mass (left panel) and mass column (right panel). The simulation assumes a contaminant vaporization rate one-tenth that of octadecane (see text).

5. SUMMARY

Although the *Chandra* contamination-migration model (CCMM) is a useful tool for assessing relative efficacy of various bake-out scenarios, its utility for absolute predictions remains limited. The main factors limiting its utility are (1) incomplete knowledge of the volatility properties of the contaminants, (2) exponential propagation of temperature uncertainties onto vaporization rates; and (3) neglect of potentially important physical processes. Among these processes are (1) interaction of multiple species in determining vaporization rates, (2) surface re-distribution (especially for a liquid contaminant), and (3) dependence of OBF thermal emissivity upon thickness of the contaminating layer.

A priority for achieving more useful simulations is to constrain better the volatility properties of the molecular contaminants. Spatial gradients in the accumulation rate across the OBFs and its time dependence carry potentially useful information on the relative vaporization and deposition rates. Continued high-resolution spectroscopy of the carbon, oxygen, and fluorine K edges and their temporal changes may provide hints toward identifying the contaminant(s).

Over the past couple years, the *Chandra* Team revisited the 2004 decision[17] not to bake-out the ACIS. The increasing accumulation rate, which started about 2010 and may still be accelerating, prompted this discussion. For now, however, the Team has agreed to defer a bake-out decision until later, based upon the following considerations:

1. Despite increasing low-energy attenuation, *Chandra* continues to be quite productive scientifically.
2. The identified risks of performing an ACIS bake-out are small but not currently demonstrably negligible.
3. A bake-out might not substantially reduce contamination on the OBFs but would reduce available observing time.

ACKNOWLEDGEMENTS

The *Chandra X-ray Observatory* is operated by the Smithsonian Astrophysical Observatory (SAO) under contract to NASA Marshall Space Flight Center (MSFC). The Advanced CCD Imaging Spectrometer (ACIS) was developed by the Massachusetts Institute of Technology (MIT) and Pennsylvania State University.

REFERENCES

[1] Weisskopf, M. C., "The Chandra X-Ray Observatory: progress report and highlights," SPIE 8443, 0Y 9pp (2012).

[2] Weisskopf, M. C, Aldcroft, T. L., Bautz, M., Cameron, R. A., Dewey, D., Drake, J. J., Grant, C. E., Marshall, H. L., & Murray, S. S., "An overview of the performance of the Chandra X-ray Observatory," Exp. Astron. 16, 1–68 (2003).

[3] Weisskopf, M. C., Brinkman, B., Canizares, C., Garmire, G., Murray, S., & Van Speybroeck, L. P., "An overview of the performance and scientific results from the Chandra X-ray Observatory," Pub. Astron. Soc. Pacific 114, 1–24 (2002).

[4] Weisskopf, M. C., Tananbaum, H. D., Van Speybroeck, L. P., & O'Dell, S. L., "Chandra X-ray Observatory (CXO): overview," SPIE 4012, 2–16 (2000).

[5] Garmire, G. P., Bautz, M. W., Ford, P. G., Nousek, J. A., & Ricker, G. R., Jr., "Advanced CCD Imaging Spectrometer (ACIS) instrument on the Chandra X-ray Observatory," SPIE 4851, 28–44 (2003).

[6] Grant, C. E., Bautz, M. W., Ford, P. G., & Plucinsky, P. P., "Fifteen years of the Advanced CCD Imaging Spectrometer," SPIE 9144, 3Q 10pp (2014).

[7] Plucinsky, P. P., Schulz, N. S., Marshall, H. L., Grant, C. E., Chartas, G., Sanwal, D., Teter, M., Vikhlinin, A. A., Edgar, R. J., Wise, M. W., Allen, G. E., Virani, S. N., DePasquale, J. M., & Raley, M. T., "Flight spectral response of the ACIS instrument," SPIE 4851, 89–100 (2003).

[8] DePasquale, J. M., Plucinsky, P. P., Vikhlinin, A. A., Marshall, H. L., Schulz, N. S., & Edgar, R. J., "Verifying the ACIS contamination model with 1E0102.2-7219," SPIE 5501, 328-338 (2004).

[9] Marshall, H. L., Tennant, A., Grant, C. E., Hitchcock, A. P., O'Dell, S. L., & Plucinsky, P. P., "Composition of the Chandra ACIS contaminant," SPIE 5165, 497–508 (2004).

[10] O'Dell, S. L., Swartz, D. A., Plucinsky, P. P., Freeman, M. A., Markevitch, M. L., Vikhlinin, A. A., Chen, K. C., Giordano, R. J., Knollenberg, P. J., Morris, P. A., Tran, H., Tice, N. W., & Anderson, S. K., "Modeling contamination migration on the Chandra X-ray Observatory," SPIE 5898, 313–324 (2005).

[11] O'Dell, S. L., Swartz, D. A., Tice, N. W., Plucinsky, P. P., Grant, C. E., Marshall, H. L., Vikhlinin, A., & Tennant, A. F., "Modeling contamination migration on the Chandra X-ray Observatory II," SPIE 8859, 0F 12pp (2013).

[12] O'Dell, S. L., Swartz, D. A., Tice, N. W., Plucinsky, P. P., Grant, C. E., Marshall, H. L., Vikhlinin, A., Tennant, A. F., and Dahmer, M. T. "Modeling contamination migration on the Chandra X-ray Observatory III," SPIE 9601, 07 13pp (2015).

[13] Plucinsky, P. P., Bogdan, A., Germain, G., & Marshall, H. L., "The evolution of the ACIS contamination layer over the 16-year mission of the Chandra X-ray Observatory," SPIE 9905, 44 15pp (2016).

[14] Marshall, H. L., Bogdan, A., & Plucinsky, P. P., "An update to the Chandra ACIS contamination model," SPIE 10397, these proceedings (2017).

[15] Monmeyran, C., Patel, N. S., Bautz, M. W., Grant, C. E., Prigozhin, G. Y., Agarwal, A., & Kimerling, L. C., "Annealing bounds to prevent further Charge Transfer Inefficiency increase of the Chandra X-ray CCDs," NIMPB 389, 23–27 (2016).

[16] Acree, W., Jr., & Chickos, J. S., "Phase transition enthalpy measurements of organic and organometallic compounds. Sublimation, vaporization, and fusion enthalpies from 1880 to 2010," J. Phys. Chem. Ref. Data 39, 043101 942pp (2010).

[17] Plucinsky, P. P., O'Dell, S. L., Tice, N. W., Swartz, D. A., Bautz, M. W., DePasquale, J. M., Edgar, R. J., Garmire, G. P., Giordano, R., Grant, C. E., Knollenberg, P., Kissel, S., LaMarr, B., Logan, R., Mach, M., Marshall, H. L., McKendrick, L., Prigozhin, G. Y., Schwartz, D., Schulz, N. S., Shropshire, D., Trinh, T., Vikhlinin, A. A., & Virani, S. N., "An evaluation of a bake-out of the ACIS instrument on the Chandra X-Ray Observatory," SPIE 5488, 251–263 (2004).